THE SIZE-DEPENDENT ELECTROMECHANICAL COUPLING RESPONSE IN CIRCULAR MICRO-PLATE DUE TO FLEXOELECTRICITY

X. Ji **A.-Q. Li***

School of Mechanical & Automotive Engineering
Qilu University of Technology
Jinan, China

School of Mechanical Engineering
Key Laboratory of High Efficiency and Clean Mechanical Manufacture
Shandong University
Jinan, China

ABSTRACT

Flexoelectricity, the coupling of strain gradient to polarization, enhances the properties of piezoelectric response desirable for advanced MEMS dramatically even in centrosymmetric dielectrics. In this paper, the general formulations of the flexoelectric couple stress theory presented by Hadjesfandiari in orthogonal curvilinear coordinate system are derived, and are then specified for the case of cylindrical coordinates. A size-dependent flexoelectric model of circular plate is established based on the current formulations in cylindrical coordinates. The governing equations, boundary conditions and initial conditions are derived by applying Hamilton's principle. The static bending and free vibration problems of a simply supported axisymmetric circular plate are carried out to illustrate the applicability of the present model. Numerical results reveal that a homogeneous electric field between the up and down surfaces of the circular plate is induced indeed. The generated deflection, induced voltage and natural frequency show obvious size effect, but the size effect is almost diminishing as the thickness of the plate is far greater than the material length scale parameter. As the increase of the flexoelectric coefficient, the induced voltage increases evidently and the generated deflection and the natural frequency increase weakly.

Keywords: Circular micro-plate, Flexoelectricity, Couple stress, Size effect.

1. INTRODUCTION

Piezoelectricity is inherent only in noncentrosymmetric materials, but a piezoelectric response can also be found in centrosymmetric dielectrics [1]. A nonuniform strain field or the presence of the strain gradient can locally break the inversion symmetry and induce polarization even in centrosymmetric dielectrics [2]. This phenomenon is termed as flexoelectricity which is the coupling between polarization and strain gradients [3]. Flexoelectricity is one of the fundamental properties allowed by symmetry for all insulators. And the flexoelectric-type piezoelectric composites offer an alternative avenue for the development of electromechanical coupling components in MEMS (Micro-electromechanical Systems) [4]. Therefore, flexoelectricity stimulates a surge of interests of researchers.

Strain gradients play a significant role in micron scales. The mechanical behaviors of micro-components have shown obvious size effect for metals, polymers and polysilicon, experimentally [5-8] and theoretically [9-14]. Further, for the dielectrics, the mechanical strain gradient is equivalent to internal electric field [15]. Due to the scaling of the strain gradients with structural feature size, flexoelectricity is expected to show a strong size dependency which have been observed in many experiments. The strain gradient induced polarization in single crystals of paraelectric $SrTiO_3$ has been measured by Zubko *et al*. [1]. Fu *et al*. confirmed the piezoelectric performance of composites fabricated by using certain non-piezoelectric components with a texture symmetry would be enhanced with their reduced sizes [4]. The scaling effect of flexoelectricity was studied by Huang *et al*. using BST micro-cantilever with its thickness down to 30 μm [16]. Li *et al*. investigated the flexoelectric effect in BZN/Ag composite where the structure symmetry permitted no macro-piezoelectricity and measured its flexoelectric coefficient [17]. In addition, for the apolar α-phase PVDF film, the flexoelectric effects have been detected under elastic tensile stretching condition with trapezoid shape [18] and bending condition with rectangle shape [19], respectively. Due to neglecting the coupling of strain gradients to polarization, the classical piezoelectric theory fails to capture the size-dependent

* Corresponding author (lianqingcool@126.com)

DOI : 10.1017/jmech.2016.104
Copyright © 2016 The Society of Theoretical and Applied Mechanics
https://doi.org/10.1017/jmech.2016.104 Published online by Cambridge University Press

flexoelectric phenomenon. Thus, the flexoelectric theories have been proposed to account for the size-dependent flexoelectric effect.

The size-dependent flexoelectric theories are developed from strain gradient theories which have achieved giant success in predicting the size effect phenomena in micro-structures. In general, according to the deformation metrics used, the strain gradient theories can be classified into couple stress theories and general strain gradient theories. In the couple stress theories [20-22], only the rotation gradients, the skew-symmetric part of the second order deformation gradients, are treated as the higher-order deformation metrics and, accordingly, two higher-order material constants are introduced in addition to the conventional Lame constants. Further, in the general strain gradient theories, the second order deformation gradients (the first order strain gradients) are regarded as the higher-order deformation metrics, and five additional higher-order material constants are involved [23]. However, the application of these theories is limited as it requires the formidable task of determining, theoretically or experimentally, five additional material constants for general strain gradient theory and two additional material constants for couple stress theory. In view of simplicity, the strain gradient theories are reduced by introducing an additional equilibrium of moments of couples to govern the behavior of higher-order stresses, and then the skew-symmetric part of the rotation gradients is ignored to formulate the modified couple stress theory with only one higher-order material constant [24] and strain gradient elastic theory with three higher-order material constants [5]. However, the mechanical effect of the moment couple is unable to be comprehended for the free character of moment vectors. In addition, the strain gradient theory with three higher-order material constants is still limited in engineering applications as three higher-order material constants are still very difficult to be determined experimentally. Actually, the three higher-order material constants are always taken the same for the same materials in previous research. Recently, however, by considering true continuum kinematical displacement and rotation, Hadjesfandiari and Dargush demonstrated the diagonal components of curvature tensor represent the torsion of the fibers along corresponding coordinate directions, while the off-diagonal components represent the curvature of these fibers in planes parallel to coordinate planes. The suitable measure of curvature must be a tensor measuring pure curvature of an arbitrary element dx_i. Hence, in this tensor, the diagonal components cannot appear [25]. Thus, they presented the consistent couple stress theory by adopting the skew-symmetric part of the rotation gradients as the curvature tensor.

On the basis of the strain gradient theories, the size-dependent flexoelectric theories containing the electromechanical coupling are proposed. In the framework of the couple stress theory, a size-dependent piezoelectric theory with rotation gradient effect has been presented by Wang *et al*. [26]. From the general strain gradient theory, Liang and Shen formulated a theory including the coupling between strain gradient and polarization to describe the size-dependent flexoelectric effect in Bernoulli-Euler beam [27]. Moreover, a flexoelectric theory even concerning the strain/electric field gradient with the surface and electrostatic force effect has been established by Shen and Hu [28]. However, these theories suffer from their dependence on underlying inaccurate enough strain gradient theories which have been mentioned above. Therefore, Hajesfandiari [29] proposed a size- dependent flexoelectric theory by considering the coupling of the polarization to the mean curvature tensor based on their couple stress theory [25].

According to the flexoelectric theories, the size-dependent flexoelectric effect have been analyzed in micro-structures. The influence of the flexoelectric effect on the static bending and free vibration of a simply supported Timoshenko beam was investigated by Yan and Jiang [30]. The first order strain gradient effects in micro piezoelectric-bimorph beam and circular plate were analyzed by Hu *et al*. [31] and Wang *et al*. [32], respectively, by considering the first order strain gradient terms in the energy density functions. In addition, Li *et al*. have developed a three-layer Bernoulli-Euler beam model with flexoelectricity to capture the size-dependent flexoelectric effect in its static bending and free vibration problems [33]. Similarly, because of the widely applications of circular plate in MEMS as sensors, resonators and actuators, it is essential to predict the properties of its size-dependent electromechanical coupling response.

Therefore, this paper aims to develop a flexoelectric circular plate model to capture the size-dependent flexoelectricity in isotropic dielectrics based on the theory presented by Hadjesfandiari [29]. The current paper is organized as following. In the next section, the flexoelectric couple stress theory is reviewed and its formulations in orthogonal curvilinear coordinates, especially in cylindrical coordinates, are derived. Then, the size-dependent flexoelectric circular plate model is established. The governing equations, boundary conditions and initial conditions are derived according to the Hamilton's principle in section 3. Afterward, the static bending and free vibration problems of a simply supported axisymmetric circular plate are analyzed in section 4 and 5, respectively. Finally, conclusions are summarized in section 6.

2. FLEXOELECTRIC COUPLE STRESS THEORY

2.1 Review of Flexoelectric Couple Stress Theory in RectangularCoordinates

According to the flexoelectric couple stress theory proposed by Hadjesfandiari [29], the size-dependent flexoelectric response is related to the skew-symmetrical part of the rotation gradient called the mean curvature tensor. For isotropic materials, though the disappearance of piezoelectric effect, the rotation gradient can also induce polarization, which is known as flexoelectric effect in some circles. The coupling between electric field and mean curvature vectors plays an important role in the electromechanical coupling. Then the electro-

https://doi.org/10.1017/jmech.2016.104 Published online by Cambridge University Press

mechanical enthalpy is expressed as,

$$H=\frac{1}{2}\lambda\varepsilon_{ii}\varepsilon_{jj}+\mu\varepsilon_{ij}\varepsilon_{ij}+8\mu l^2\kappa_i\kappa_i-\frac{1}{2}\varepsilon E_iE_i-4fE_i\kappa_i, \quad (1)$$

in which λ and μ are the Lame constants, l is the independent material length scale parameter, ε is the permittivity, f is the flexoelectric coefficient. The strain tensor ε_{ij}, the mean curvature vector κ_i, and the electric field vector E_i are defined, respectively, as

$$\varepsilon_{ij}=\frac{1}{2}(u_{i,j}+u_{j,i}) \quad (2)$$

$$\kappa_i=\frac{1}{4}(u_{j,ij}-u_{i,jj}) \quad (3)$$

$$E_i=-\phi_{,i} \quad (4)$$

where u_i is the displacement vector and ϕ is the electric potential.

2.2 Flexoelectric Couple Stress Theory in Orthogonal Curvilinear Coordinates

In this section, the formulations of flexoelectric couple stress theory in orthogonal curvilinear coordinates will be derived. In orthogonal curvilinear coordinates, the coordinates are q^i and the partial differentiation symbol is denoted as (;). The Lame coefficient H_i is defined as,

$$H_i=\sqrt{g_{ii}}, \quad (5)$$

in which g_{ij} is the metric tensor. Based on the relationship between the tensor components and its physical components, the physical components of displacement gradient $u_{i;j}$ and higher-order displacement gradient $u_{i;jk}$ can be expressed as

$$u_{(i;j)}=\frac{1}{H_iH_j}\left[\frac{\partial}{\partial q^j}(H_iu_{(i)})-H_ku_{(k)}\Gamma^k_{ij}\right], \quad (6)$$

$$u_{(i;jk)}=\frac{1}{H_iH_jH_k}\left[\frac{\partial}{\partial q^k}(u_{(i;j)}H_iH_j)-H_iH_ru_{(i;r)}\Gamma^r_{jk}-H_rH_ju_{(r;j)}\Gamma^r_{ik}\right], \quad (7)$$

in which Γ^k_{ij} are the Christoffel symbols of the second kind. $u_{(i)}$, $u_{(i;j)}$ and $u_{(i;jk)}$ are the physical components of displacement vector u_i, displacement gradient $u_{i;j}$ and higher-order displacement gradient $u_{i;jk}$, respectively. The physical components of strain tensor ε_{ij}, the mean curvature vector κ_i, and the electric field vector E_i are written as

$$\varepsilon_{(ij)}=\frac{1}{2}(u_{(i;j)}+u_{(j;i)}), \quad (8)$$

$$\kappa_{(i)}=\frac{1}{4H_i}[u_{(j;ij)}-u_{(i;jj)}], \quad (9)$$

$$E_{(i)}=-\frac{1}{H_i}\frac{\partial\phi}{\partial q^i}. \quad (10)$$

For the convenience of writing in the following sections, the conventional components will be used in place of the proceeding expressions for the physical components of all tensors and vectors [34, 35], e.g., using the common expression u_i in place of the component form $u_{(i)}$, ε_{ij} for $\varepsilon_{(ij)}$, κ_i for $\kappa_{(i)}$, E_i for $E_{(i)}$, etc.

2.3 Flexoelectric Couple Stress Theory in Cylindrical Coordinates

In the cylindrical coordinates, the coordinates

$$q^1=r, \quad q^2=\theta, \quad q^3=z, \quad (11)$$

can be related to the Cartesian coordinates (x, y, z) by

$$x=r\cos\theta, \quad y=r\sin\theta, \quad z=z. \quad (12)$$

The Lame coefficients H_i have the following components,

$$H_1=1, \quad H_2=r, \quad H_3=1, \quad (13)$$

and the Christoffel symbols of the second kind have the following values,

$$\Gamma^1_{22}=-r, \quad \Gamma^2_{12}=\Gamma^2_{21}=\frac{1}{r}. \quad (14)$$

From Eq. (8), the strain components in cylindrical coordinate are obtained by using Eqs. (13)-(14).

$$\varepsilon_{rr}=\frac{\partial u_r}{\partial r}, \quad \varepsilon_{\theta\theta}=\frac{\partial u_\theta}{r\partial\theta}+\frac{u_r}{r}, \quad \varepsilon_{zz}=\frac{\partial u_z}{\partial z}, \quad (15)$$

$$\varepsilon_{r\theta}=\frac{1}{2}\left(\frac{\partial u_\theta}{\partial r}+\frac{\partial u_r}{r\partial\theta}-\frac{u_\theta}{r}\right), \quad \varepsilon_{rz}=\frac{1}{2}\left(\frac{\partial u_z}{\partial r}+\frac{\partial u_r}{\partial z}\right), \quad \varepsilon_{\theta z}=\frac{1}{2}\left(\frac{\partial u_z}{r\partial\theta}+\frac{\partial u_\theta}{\partial z}\right). \quad (16)$$

Substituting Eqs. (13)-(14) into Eq. (9), the mean curvature components in cylindrical coordinate are

$$\kappa_r=\frac{1}{4}\left[\frac{\partial^2u_\theta}{r\partial r\partial\theta}+\frac{\partial^2u_z}{\partial r\partial z}-\frac{\partial^2u_r}{r^2\partial\theta^2}-\frac{\partial^2u_r}{\partial z^2}+\frac{\partial u_\theta}{r^2\partial\theta}\right], \quad (17)$$

$$\kappa_\theta=\frac{1}{4r}\left[\frac{\partial^2u_r}{r\partial r\partial\theta}-\frac{\partial^2u_\theta}{\partial r^2}-\frac{\partial^2u_\theta}{\partial z^2}+\frac{\partial^2u_z}{r\partial\theta\partial z}-\frac{\partial u_r}{r^2\partial\theta}-\frac{\partial u_\theta}{r\partial r}+\frac{u_\theta}{r^2}\right], \quad (18)$$

$$\kappa_z=\frac{1}{4}\left[\frac{\partial^2u_r}{\partial r\partial z}+\frac{\partial^2u_\theta}{r\partial z\partial\theta}-\frac{\partial^2u_z}{r^2\partial\theta^2}-\frac{\partial^2u_z}{\partial r^2}+\frac{\partial u_r}{r\partial z}-\frac{\partial u_z}{r\partial r}\right]. \quad (19)$$

The electric field components in cylindrical coordinate can also be obtained by substituting Eqs. (13)-(14) into Eq. (10).

$$E_r=-\phi_{,r}, \quad E_\theta=-\frac{\phi_{,\theta}}{r}, \quad E_z=-\phi_{,z}. \quad (20)$$

https://doi.org/10.1017/jmech.2016.104 Published online by Cambridge University Press

3. THE GOVERNING EQUATIONS AND BOUNDARY CONDITIONS OF FLEXOELECTRIC CIRCULAR MICRO-PLATE

Consider an isotropic homogeneous flexoelectric thin circular plate of thickness h and diameter $2a$, subjected to transverse load $q(r, \theta, t)$ as shown in Fig. 1. A cylindrical coordinate system is adopted, where r-θ plane coincides with the neutral plane. According to the Kirchhoff assumption for thin plate, the displacement components can be taken as [36]

$$u_r = -z\frac{\partial w}{\partial r}, \quad u_\theta = -z\frac{\partial w}{r\partial \theta}, \quad u_z = w(r,\theta,t), \tag{21}$$

where u_r, u_θ, u_z, are the r-, θ-, z-components of the displacement vector and t denotes time. The poling direction is assumed to be in the z-direction [36, 37]. Hence, the electric potential can be considered as

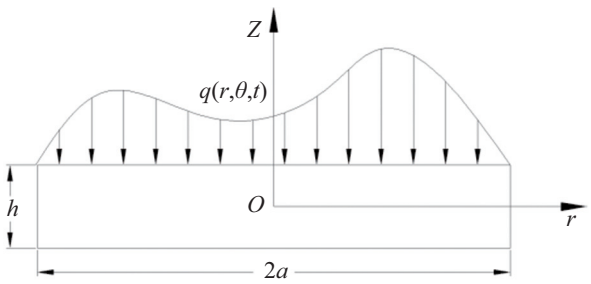


Fig. 1 Schematic of a circular micro-plate with distributed load.

$$\phi = \phi(z,t) \tag{22}$$

Substituting Eqs. (21)-(22) into Eqs. (15)-(20), the non-zero strain, mean curvature and electric field components are written as

$$\varepsilon_{rr} = -z\frac{\partial^2 w}{\partial r^2}, \quad \varepsilon_{\theta\theta} = -z\left(\frac{\partial^2 w}{r^2\partial\theta^2} + \frac{\partial w}{r\partial r}\right), \quad \varepsilon_{r\theta} = z\left(\frac{\partial w}{r^2\partial\theta} - \frac{\partial^2 w}{r\partial r\partial\theta}\right), \tag{23}$$

$$\kappa_z = -\frac{1}{2}\left(\frac{\partial^2 w}{\partial r^2} + \frac{\partial^2 w}{r^2\partial\theta^2} + \frac{\partial w}{r\partial r}\right), \tag{24}$$

$$E_z = -\frac{\partial \phi}{\partial z}. \tag{25}$$

From Eq. (1), the electromechanical enthalpy density of Kirchhoff circular plate in cylindrical coordinate is simplified to

$$\begin{aligned} H = {} & \frac{1}{2}\frac{Ez^2}{1-\nu^2}\left[\left(\frac{\partial^2 w}{\partial r^2}\right)^2 + \left(\frac{\partial^2 w}{r^2\partial\theta^2}\right)^2 + \left(\frac{\partial w}{r\partial r}\right)^2 + 2\nu\frac{\partial^2 w}{\partial r^2}\frac{\partial^2 w}{r^2\partial\theta^2} + 2\nu\frac{\partial w}{r\partial r}\frac{\partial^2 w}{\partial r^2} + 2\frac{\partial w}{r\partial r}\frac{\partial^2 w}{r^2\partial\theta^2}\right] \\ & + 2\mu l^2\left[\left(\frac{\partial^2 w}{\partial r^2}\right)^2 + \left(\frac{\partial^2 w}{r^2\partial\theta^2}\right)^2 + \left(\frac{\partial w}{r\partial r}\right)^2 + 2\frac{\partial^2 w}{\partial r^2}\frac{\partial^2 w}{r^2\partial\theta^2} + 2\frac{\partial^2 w}{r^2\partial\theta^2}\frac{\partial w}{r\partial r} + 2\frac{\partial^2 w}{\partial r^2}\frac{\partial w}{r\partial r}\right] \\ & + 2\mu z^2\left[\left(\frac{\partial w}{r^2\partial\theta}\right)^2 - 2\frac{\partial w}{r^2\partial\theta}\frac{\partial^2 w}{r\partial r\partial\theta} + \left(\frac{\partial^2 w}{r\partial r\partial\theta}\right)^2\right] - \frac{1}{2}\varepsilon\left(\frac{\partial\phi}{\partial z}\right)^2 - 2f\frac{\partial\phi}{\partial z}\left(\frac{\partial^2 w}{r^2\partial\theta^2} + \frac{\partial^2 w}{\partial r^2} + \frac{\partial w}{r\partial r}\right), \end{aligned} \tag{26}$$

in which E is the Young's modulus and ν is the Poisson ratio. Then, by integrating the electromechanical enthalpy density on the total circular plate, the total electromechanical enthalpy can be written as

$$\Pi = \int_0^a\int_0^{2\pi}\int_{-h/2}^{h/2} H r d\theta dr dz. \tag{27}$$

Considering the bending rigidity of thin circular plate in the traditional elasticity theory,

$$D = \frac{Eh^3}{12(1-\nu^2)}, \tag{28}$$

the total electromechanical enthalpy can be simplified to

$$\Pi = \int_0^a\int_0^{2\pi} F d\theta dr - \int_0^a\int_0^{2\pi}\int_{-h/2}^{h/2} S d\theta dr dz - \frac{1}{2}\varepsilon\pi a^2\int_{-h/2}^{h/2}\left(\frac{\partial\phi}{\partial z}\right)^2 dz \tag{29}$$

https://doi.org/10.1017/jmech.2016.104 Published online by Cambridge University Press

in which F and S are given as

$$F=\frac{1}{2}D\left[r\left(\frac{\partial^2 w}{\partial r^2}\right)^2+\frac{1}{r^3}\left(\frac{\partial^2 w}{\partial\theta^2}\right)^2+\frac{1}{r}\left(\frac{\partial w}{\partial r}\right)^2+\frac{2\nu}{r}\frac{\partial^2 w}{\partial r^2}\frac{\partial^2 w}{\partial\theta^2}+2\nu\frac{\partial w}{\partial r}\frac{\partial^2 w}{\partial r^2}+\frac{2}{r^2}\frac{\partial w}{\partial r}\frac{\partial^2 w}{\partial\theta^2}\right]$$
$$+2\mu l^2 h\left[\frac{1}{r^3}\left(\frac{\partial^2 w}{\partial\theta^2}\right)^2+r\left(\frac{\partial^2 w}{\partial r^2}\right)^2+\frac{1}{r}\left(\frac{\partial w}{\partial r}\right)^2+\frac{2}{r}\frac{\partial^2 w}{\partial r^2}\frac{\partial^2 w}{\partial\theta^2}+\frac{2}{r^2}\frac{\partial^2 w}{\partial\theta^2}\frac{\partial w}{\partial r}+2\frac{\partial^2 w}{\partial r^2}\frac{\partial w}{\partial r}\right] \tag{30}$$
$$+\frac{1}{6}\mu h^3\left[\frac{1}{r^3}\left(\frac{\partial w}{\partial\theta}\right)^2-\frac{2}{r^2}\frac{\partial w}{\partial\theta}\frac{\partial^2 w}{\partial r\partial\theta}+\frac{1}{r}\left(\frac{\partial^2 w}{\partial r\partial\theta}\right)^2\right],$$

$$S=2fr\frac{\partial\phi}{\partial z}\left(\frac{\partial^2 w}{r^2\partial\theta^2}+\frac{\partial^2 w}{\partial r^2}+\frac{\partial w}{r\partial r}\right). \tag{31}$$

The variation of the total electromechanical enthalpy is derived as

$$\delta\Pi=\int_0^a\int_0^{2\pi}[r(D+4\mu l^2h)\nabla^2\nabla^2 w]\delta w d\theta dr+\varepsilon\pi a^2\int_{-h/2}^{h/2}\frac{\partial^2\phi}{\partial z^2}\delta\phi dz$$
$$-\left[\int_0^{2\pi}r\left[(D+4\mu l^2h)\left(\frac{\partial^3 w}{\partial r^3}+\frac{\partial^3 w}{r^2\partial r\partial\theta^2}-\frac{\partial w}{r^2\partial r}+\frac{\partial^2 w}{r\partial r^2}-2\frac{\partial^2 w}{r^3\partial\theta^2}\right)\right.\right.$$
$$\left.+D(1-\nu)\left(\frac{\partial^3 w}{r^2\partial r\partial\theta^2}-\frac{\partial^2 w}{r^3\partial\theta^2}\right)\right]\delta w d\theta\Bigg]_0^a-\left[\int_0^a\left[(D+4\mu l^2h)\left(\frac{\partial^3 w}{r^3\partial\theta^3}+\frac{\partial^3 w}{r\partial r^2\partial\theta}+\frac{\partial^2 w}{r^2\partial r\partial\theta}\right)\right.\right.$$
$$\left.+D(1-\nu)\left(\frac{\partial^3 w}{r\partial r^2\partial\theta}-2\frac{\partial^2 w}{r^2\partial r\partial\theta}+2\frac{\partial w}{r^3\partial\theta}\right)\right]\delta w dr\Bigg]_0^{2\pi} \tag{32}$$
$$+\left[\int_0^{2\pi}r\left[(D+4\mu l^2h)\frac{\partial^2 w}{\partial r^2}+(D\nu+4\mu l^2h)\left(\frac{\partial^2 w}{r^2\partial\theta^2}+\frac{\partial w}{r\partial r}\right)-2f\left(\phi\big|_{-h/2}^{h/2}\right)\right]\delta w_{,r}d\theta\right]_0^a$$
$$+\left[\int_0^a\frac{1}{r}\left[(D+4\mu l^2h)\left(\frac{\partial^2 w}{r^2\partial\theta^2}+\frac{\partial w}{r\partial r}\right)+(D\nu+4\mu l^2h)\frac{\partial^2 w}{\partial r^2}-2f\left(\phi\big|_{-h/2}^{h/2}\right)\right]\delta w_{,\theta}dr\right]_0^{2\pi}$$
$$-\left[\int_0^a\int_0^{2\pi}\left[2f\left(\frac{\partial^2 w}{\partial r^2}+\frac{\partial^2 w}{r^2\partial\theta^2}+\frac{\partial w}{r\partial r}\right)+\varepsilon\frac{\partial\phi}{\partial z}\right]r\delta\phi d\theta dr\right]_{-h/2}^{h/2},$$

where the Laplacian operator is

$$\nabla^2=\frac{\partial^2}{\partial r^2}+\frac{\partial}{r\partial r}+\frac{\partial^2}{r^2\partial\theta^2}. \tag{33}$$

On the other hand, the variation of work done by the transverse load $q(r, \theta, t)$ is given as,

$$\delta W=\int_0^a\int_0^{2\pi}q\delta w r dr d\theta, \tag{34}$$

and the variation of the kinetic energy can be written as,

$$\delta T=\delta\left[\frac{1}{2}\rho h\int_0^a\int_0^{2\pi}\dot{w}^2 r dr d\theta\right]. \tag{35}$$

where ρ is the material density.

Therefore, on the basis of the Hamilton's principle,

$$\delta\int_{t_1}^{t_2}(T-\Pi+W)dt=0, \tag{36}$$

with t_1 and t_2 denoting different time, respectively, the governing equations are derived as,

https://doi.org/10.1017/jmech.2016.104 Published online by Cambridge University Press

$$(D+4\mu l^2 h)\nabla^2\nabla^2 w+\ddot{w}\rho h=q, \tag{37}$$

$$\frac{\partial^2\phi}{\partial z^2}=0, \tag{38}$$

and the boundary conditions are,

$$\left[(D+4\mu l^2 h)\left(\frac{\partial^3 w}{\partial r^3}+\frac{\partial^3 w}{r^2\partial r\partial\theta^2}-\frac{\partial w}{r^2\partial r}+\frac{\partial^2 w}{r\partial r^2}-2\frac{\partial^2 w}{r^3\partial\theta^2}\right)+D(1-\nu)\left(\frac{\partial^3 w}{r^2\partial r\partial\theta^2}-\frac{\partial^2 w}{r^3\partial\theta^2}\right)\right]\delta w|_0^a=0, \tag{39}$$

$$\left[(D+4\mu l^2 h)\left(\frac{\partial^3 w}{r^3\partial\theta^3}+\frac{\partial^3 w}{r\partial r^2\partial\theta}+\frac{\partial^2 w}{r^2\partial r\partial\theta}\right)+D(1-\nu)\left(\frac{\partial^3 w}{r\partial r^2\partial\theta}-2\frac{\partial^2 w}{r^2\partial r\partial\theta}+2\frac{\partial w}{r^3\partial\theta}\right)\right]\delta w|_0^{2\pi}=0, \tag{40}$$

$$\left[(D+4\mu l^2 h)\frac{\partial^2 w}{\partial r^2}+(D\nu+4\mu l^2 h)\left(\frac{\partial^2 w}{r^2\partial\theta^2}+\frac{\partial w}{r\partial r}\right)-2f\left(\phi|_{-h/2}^{h/2}\right)\right]\delta w_{,r}|_0^a=0,, \tag{41}$$

$$\left[(D+4\mu l^2 h)\left(\frac{\partial^2 w}{r^2\partial\theta^2}+\frac{\partial w}{r\partial r}\right)+(D\nu+4\mu l^2 h)\frac{\partial^2 w}{\partial r^2}-2f\left(\phi|_{-h/2}^{h/2}\right)\right]\delta w_{,\theta}|_0^{2\pi}=0, \tag{42}$$

$$\left[2f\left(r\frac{\partial w}{\partial r}\right)_0^a+\int_0^a 2f\frac{\partial^2 w}{r\partial\theta^2}dr+\frac{a^2}{2}\varepsilon\frac{\partial\phi}{\partial z}\right]\delta\phi|_{-h/2}^{h/2}=0. \tag{43}$$

$$\rho h\dot{w}\delta w|_{t_1}^{t_2}=0 \tag{44}$$

When the induced electric field is ignored, the governing equations and boundary conditions reduce to that of the pure couple stress circular plate model.

4. STATIC BENDING OF AN AXISYMMETRIC SIMPLY SUPPORTED CIRCULAR PLATE

Consider an axisymmetric simply supported circular plate subjected to a uniformly distributed load q_0. Then, the plate parameters such as transverse deflection w will only depend upon the radial position r. In this case, for the static bending problem, the governing equations in Eqs. (37) and (38) reduce to,

$$(D+4\mu l^2 h)\left(\frac{d^2}{dr^2}+\frac{1}{r}\frac{d}{dr}\right)\left(\frac{d^2 w}{dr^2}+\frac{1}{r}\frac{dw}{dr}\right)=q_0, \tag{45}$$

$$\frac{d^2\phi}{dz^2}=0. \tag{46}$$

While, considering the arbitrariness of δw, $\delta w_{,r}$ and $\delta\phi$, the boundary conditions at $r=a$ can be reduced from Eqs. (39) and (41),

$$w|_{r=a}=0, \tag{47}$$

$$\left[(D+4\mu l^2 h)\frac{d^2 w}{dr^2}+(D\nu+4\mu l^2 h)\frac{dw}{rdr}-2f\left(\phi|_{-h/2}^{h/2}\right)\right]\Bigg|_{r=a}=0, \tag{48}$$

and the boundary conditions at the top and bottom can be rewritten from Eq. (43), respectively,

$$\left[2f\left(r\frac{\partial w}{\partial r}\right)\Big|_0^a+\frac{a^2}{2}\varepsilon\frac{\partial\phi}{\partial z}\right]\Bigg|_{z=h/2}=0, \tag{49}$$

$$\left[2f\left(r\frac{\partial w}{\partial r}\right)\Big|_0^a+\frac{a^2}{2}\varepsilon\frac{\partial\phi}{\partial z}\right]\Bigg|_{z=-h/2}=0. \tag{50}$$

According to the governing equations Eqs. (45) and (46) subjected to the boundary conditions Eqs. (47)-(50), the deflection is solved as,

$$w=C_1\ln r+C_2 r^2\ln r+C_3 r^2+C_4+\frac{q_0 r^4}{64(D+4\mu l^2 h)}, \tag{51}$$

and the induced electric potential, by considering the electric potential on the subface equal zero due to its relativity, is given as,

$$\phi=C_5\left(z+h/2\right), \tag{52}$$

in which coefficients C_1 and C_2 equal zero due to the finite deformation of the circular plate at its center and the coefficients C_3, C_4 and C_5 are

$$C_3=-\frac{q_0 a^2}{32(D+4\mu l^2 h)}\frac{D(3+\nu)+16\mu l^2 h+\dfrac{8hf^2}{\varepsilon}}{D(1+\nu)+8\mu l^2 h+\dfrac{8hf^2}{\varepsilon}}, \tag{53}$$

https://doi.org/10.1017/jmech.2016.104 Published online by Cambridge University Press

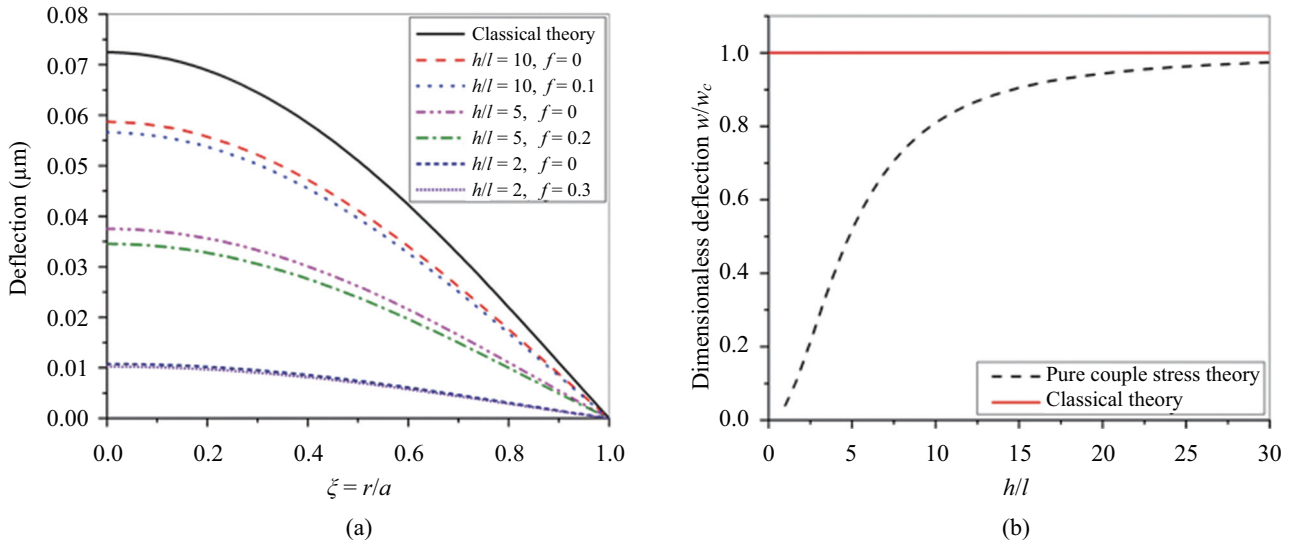


Fig. 2 The size-dependent deflection (a) the distribution of generated deflection along the radius direction (b) the size effect of dimensionless deflection at the central point of circular plate.

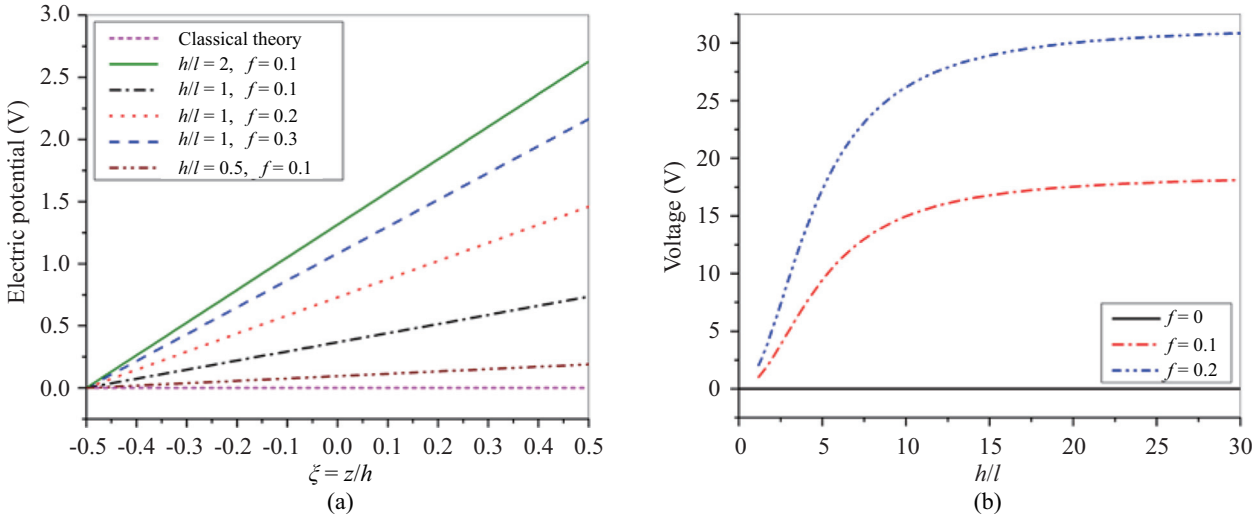


Fig. 3 The size-dependent flexoelectricity (a) the distribution of induced electric potential along the thickness direction (b) the size effect of induced voltage.

$$C_4 = \frac{q_0 a^4}{64(D+4\mu l^2 h)} \frac{D(5+\nu)+24\mu l^2 h+\dfrac{8hf^2}{\varepsilon}}{D(1+\nu)+8\mu l^2 h+\dfrac{8hf^2}{\varepsilon}}, \tag{54}$$

$$C_5 = \frac{f}{2\varepsilon} \frac{q_0 a^2}{D(1+\nu)+8\mu l^2 h+\dfrac{8hf^2}{\varepsilon}}. \tag{55}$$

When flexoelectric coefficient f equals zero, the flexoelectric effect disappears and the deflection reduces to that of the pure couple stress theory, w_p. Further, when both the material length scale parameter l and flexoelectric coefficient f are equal to zero, the deflection reduces to that of classical theory, w_c.

To illustrate the solutions of the simply supported circular plate, some numerical results are shown as Figs. 2 and 3 under the uniformly distributed load q_0 = 20 μN. The geometry of the circular plate is set as a = 5 μm, h = 1 μm. $BaTiO_3$ is taken as the example material with its Young's modulus and dielectric constant given as E = 120 GPa, $\varepsilon = 8.85 \times 10^{-3}$ PF/μm, respectively. From the curves in Fig. 2, it can be seen that the generated deflection of the bending circular plate shows obvious size effect, which is similar to that predicted by other strain gradient theories. When the thickness of the circular plate is comparable to the material length scale parameter, the deflection of the circular plate is far smaller than that of the classical theory. However, the size effect is almost diminishing when the thickness of circular plate is far greater than the material length scale parameter. In addition, the generated deflection of the circular plate decreases due to the influence of the flexoelectric effect

https://doi.org/10.1017/jmech.2016.104 Published online by Cambridge University Press

and the stronger the size effect, the smaller the influence of the flexoelectric effect on deflection.

Due to the strain gradient, a electric field will be induced in the circular plate. The distribution of the induced potential is shown in Fig. 3(a) and the size effect of induced voltage, the difference of induced electric potential between the up and down surfaces of the plate, can be found in Fig. 3(b). Figure 3 predicts that induced electric potential is linear along the thickness direction of the plate and its proportionality coefficient decreases evidently with the decrease of characteristic size and increases apparently as the flexoelectric coefficient increases. The size-dependent induced voltage tends to be constant as the increase of the characteristic size. When the flexoelectric coefficient equals zero, the flexoelectric process disappears.

5. FREE VIBRATION OF A SIMPLY SUPPORTED CIRCULAR PLATE

In this section, the free vibration of a simply supported circular plate is analyzed. From Eq. (37), the governing equation is obtained by neglecting the external force, expressing

$$\nabla^2\nabla^2 w+\frac{\rho h}{D+4\mu l^2 h}\ddot{w}=0. \tag{56}$$

Assuming that,

$$w(r,\theta,t)=R(r)A(\theta)\sin(\omega t+\varphi), \tag{57}$$

where ω denotes the circular frequency, φ denote the initial phase, R is a function of r alone and A is a function of θ alone. Substituting Eq. (57) into Eq. (56) yields,

$$\left(\frac{d^2R}{dr^2}+\frac{1}{r}\frac{dR}{dr}\right)A+\frac{1}{r^2}R\frac{d^2A}{d\theta^2}\pm\alpha^2RA=0, \tag{58}$$

in which the coefficient α is given by,

$$\alpha^4=\frac{\rho h}{D+4\mu l^2 h}\omega^2. \tag{59}$$

Applying the variable separation method, Eq. (58) can be rewritten as

$$\frac{\dfrac{d^2R}{dr^2}+\dfrac{1}{r}\dfrac{dR}{dr}\pm\alpha^2R}{-\dfrac{R}{r^2}}=\frac{\dfrac{d^2A}{d\theta^2}}{A}=-m^2, \tag{60}$$

and then yields two equations,

$$\frac{d^2A}{d\theta^2}+m^2A=0, \tag{61}$$

$$\frac{d^2R}{dr^2}+\frac{1}{r}\frac{dR}{dr}+\left(\pm\alpha^2-\frac{m^2}{r^2}\right)R=0, \tag{62}$$

in which the constant $m = 0, 1, 2, \ldots$.

Due to the axial symmetry of the simply circular plate, the solution of Eq. (61) is given as,

$$A(\theta)=E_m\cos m\theta. \tag{63}$$

And the solution of Eq. (62) is given as,

$$R(r)=A_mJ_m(\alpha r)+B_mI_m(\alpha r)+C_mY_m(\alpha r)+D_mK_m(\alpha r), \tag{64}$$

in which J_m and Y_m denote the Bessel functions of order m of the first and second kinds, respectively, and I_m and K_m are the modified Bessel functions of the first and second kinds, and A_m, B_m, C_m and D_m are arbitrary constants. In the case of a solid plate without hole, Y_m and K_m are inadmissible because of the singularity at $r = 0$ and Eq. (64) may be represented in the form [38],

$$R(r)=A_mJ_m(\alpha r)+B_mI_m(\alpha r). \tag{65}$$

Hence, the general solution of Eq. (56) may now be written as,

$$w(r,\theta,t)=\sum_{m=1}^{\infty}[A_mJ_m(\alpha r)+B_mI_m(\alpha r)]\cos m\theta\sin(\omega t+\varphi). \tag{66}$$

According to Eqs. (47)-(50), boundary conditions are,

$$w(a,\theta,t)=0, \tag{67}$$

$$\begin{aligned}&(D+4\mu l^2h)\frac{\partial^2w(a,\theta,t)}{\partial r^2}\\&+\left(D\nu+4\mu l^2h+\frac{8hf^2}{\varepsilon}\right)\frac{\partial w(a,\theta,t)}{a\partial r}=0.\end{aligned} \tag{68}$$

Substituting Eq. (66) into boundary conditions Eqs. (67) and (68) gives

$$A_mJ_m(\alpha a)+B_mI_m(\alpha a)=0, \tag{69}$$

$$\begin{aligned}&A_m\left[\frac{\partial^2J_m(\alpha a)}{\partial r^2}+\frac{D\nu+4\mu l^2h+\dfrac{8hf^2}{\varepsilon}}{a(D+4\mu l^2h)}\frac{\partial J_m(\alpha a)}{\partial r}\right]\\&+B_m\left[\frac{\partial^2I_m(\alpha a)}{\partial r^2}+\frac{D\nu+4\mu l^2h+\dfrac{8hf^2}{\varepsilon}}{a(D+4\mu l^2h)}\frac{\partial I_m(\alpha a)}{\partial r}\right]=0.\end{aligned} \tag{70}$$

The frequency equation is given by the condition that the homogeneous system Eqs. (69) and (70) yield nontrivial solutions for A_m and B_m, and may be written,

$$\frac{J_{m+1}(\alpha a)}{J_m(\alpha a)}+\frac{I_{m+1}(\alpha a)}{I_m(\alpha a)}-2\alpha a\frac{D+4\mu l^2h}{D(1-\nu)-\dfrac{8hf^2}{\varepsilon}}=0. \tag{71}$$

Consider the frequency coefficient $\alpha_{mn}a=\lambda_{mn}$ ($m, n = 0, 1, 2, \ldots$), then the (m, n) order natural frequency can be expressed as,

https://doi.org/10.1017/jmech.2016.104 Published online by Cambridge University Press

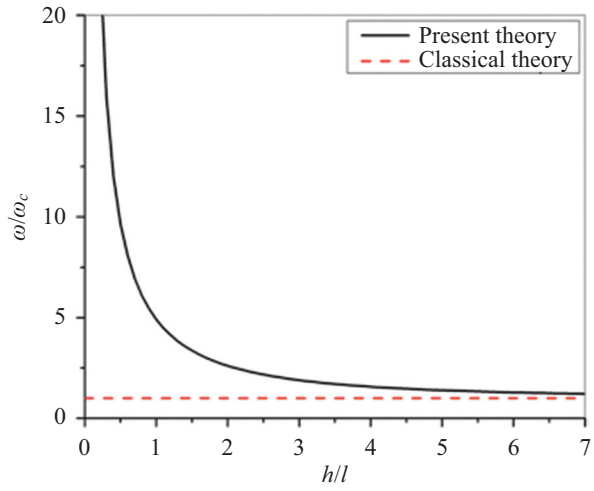


Fig. 4 The size effect of the dimensionless natural frequency.

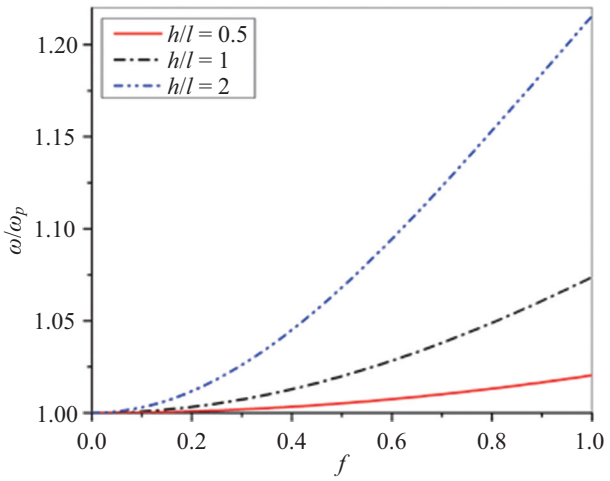


Fig. 5 The influence of the flexoelectric coefficient on the natural frequency.

$$\omega_{mn} = \frac{\lambda_{mn}^2}{a^2}\sqrt{\frac{D+4\mu l^2 h}{\rho h}}. \tag{72}$$

When flexoelectric effect is ignored by letting $f = 0$, the frequency equation Eq. (71) and the responding natural frequency Eq. (72) reduce to that of the pure couple stress theory. Further, if both the material length scale parameter l and flexoelectric coefficient f are equal to zero, the frequency equation and the responding natural frequency reduce to that of classical theory.

To illustrate the newly derived solution of the simply supported circular plate, some numerical results have been obtained for the natural frequency with $m = n = 0$. The dimensionless natural frequency ω/ω_c is shown in Fig. 4 to assess its size-dependence where ω_c denotes the natural frequency in classical theory. Besides, another dimensionless natural frequency ω/ω_p is shown in Fig. 5 to assess the influence of the flexoelectric coefficient in which ω_p is the natural frequency in pure couple stress theory. Figure 4 reveals the evident size effect of the natural frequency. The natural frequency increases significantly in comparison with the classical one when the beam thickness is less than or close to the material length scale parameter. But the size effect is almost diminishing as the thickness of the beam is far greater than the material length scale parameter. From the curves in Fig. 5, it can be found that the natural frequency increases weakly, in contrast with that of pure couple stress theory, as the increase of the flexoelectric coefficient. In addition, the dimensionless natural frequency ω/ω_p increases as the characteristic size increase due to the decrease of the natural frequency.

6. CONCLUSIONS

In this work, the flexoelectric couple stress theory presented by Hadjesfandiari is reformulated in orthogonal curvilinear coordinate system, and are then specified for the case of cylindrical coordinates. Afterwards, on the basis of the new derived formulations in cylindrical coordinates, a size-dependent flexoelectric model of circular plate is established. The governing equations, boundary conditions and initial conditions are derived according to the Hamilton's principle. The static bending and free vibration problems of a simply supported axisymmetric circular plate subjected to a uniform distributed load are carried out to illustrate the applicability of the current model. Numerical results reveal that a homogeneous electric field between the up and down surfaces of the circular plate is induced indeed due to the coupling of strain gradient to polarization without external electric field. The generated deflection, induced voltage and natural frequency show obvious size effect, but the size effect is almost diminishing as the thickness of the plate is far greater than the material length scale parameter. The generated deflection of the circular plate decreases due to the influence of the flexoelectric effect and the stronger the size effect, the smaller the influence of the flexoelectric effect on deflection. In addition, as the increase of the flexoelectric coefficient, the induced voltage increases evidently and the natural frequency increases weakly.

REFERENCES

1. Zubko, P., *et al*., "Strain-gradient-induced polarization in $SrTiO_3$ single crystals," *Physical Review Letters*, **99**, pp. 167601-1-4 (2007).
2. Majdoub, M. S., *et al*., "Enhanced size-dependent piezoelectricity and elasticity in nanostructures due to the flexoelectric effect," *Physical Review B*, **77**, pp. 125424-1-9 (2008).
3. Zubko, P., *et al*., "Flexoelectric effect in solids," *Annual Review of Materials Research*, **43**, pp. 387-421 (2013).
4. Fu, J. Y., *et al*., "Gradient scaling phenomenon in microsize flexoelectric piezoelectric composites," *Applied Physics Letters*, **91**, pp. 182910-1-3 (2007).

https://doi.org/10.1017/jmech.2016.104 Published online by Cambridge University Press

5. Lam, D. C. C., *et al*., "Experiments and theory in strain gradient elasticity," *Journal of the Mechanics and Physics of Solids*, **51**, pp. 1477-1508 (2003).
6. Chasiotis, I. and Knauss, W. G., "The mechanical strength of polysilicon films: Part 2. Size effects associated with elliptical and circular perforations," *Journal of Mechanics and Physics of Solids*, **51**, pp. 1551-1572 (2003).
7. Tang, C. and Alici, G., "Evaluation of length-scale effects for mechanical behaviour of micro- and nanocantilevers: Ⅰ. experimental determination of length-scale factors," *Journal of Physics D-Applied Physics*, **44**, pp. 335501-1-12 (2011).
8. Tang, C. and Alici, G., "Evaluation of length-scale effects for mechanical behaviour of micro- and nanocantilevers: Ⅱ. experimental verification of deflection models using atomic for microscopy," *Journal of Physics D-Applied Physics*, **44**, pp. 335502-1-7 (2011).
9. Li, A. Q., *et al*., "A size-dependent bilayered microbeam model based on strain gradient elasticity theory," *Composite Structures*, **108**, pp. 259-266 (2014).
10. Li, A. Q., *et al*., "A size-dependent model for bi-layered Kirchhoff micro-plate based on strain gradient elasticity theory," *Composite Structures*, **113**, pp. 272-280 (2014).
11. Kong, S. L., *et al*., "The size-dependent natural frequency of Bernoulli-Euler micro-beams," *International Journal of Engineering Science*, **46**, pp. 427-437 (2008).
12. Kong, S. L., *et al*., "Static and dynamic analysis of micro beams based on strain gradient elasticity theory," *International Journal of Engineering Science*, **47**, pp. 487-498 (2009).
13. Wang, B. L., *et al*., "A micro scale Timoshenko beam model based on strain gradient elasticity theory," *European Journal of Mechanics A-Solids*, **29**, pp. 591-599 (2010).
14. Wang, B. L., *et al*., "A size-dependent Kirchhoff micro-plate model based on strain gradient elasticity theory," *European Journal of Mechanics A-Solids*, **30**, pp. 517-524 (2011).
15. Ma, W. H., "A study of flexoelectric coupling associated internal electric field and stress in thin film ferroelectrics," *Physica status Solidi (b)*, **245**, pp. 761-768 (2008).
16. Huang, W. B., *et al*., "Scaling effect of flexoelectric (Ba,Sr)TiO3 microcantilevers," *Physica Status Solidi-Rapid Research Letters*, **5**, pp. 350-352 (2011).
17. Li, Y., *et al*., "Enhanced flexoelectric effect in a non-ferroelectric composite," *Applied Physics Letters*, **103**, pp. 142909-1-4 (2013).
18. Baskaran, S., *et al*., "Experimental studies on the direct flexoelectric effect in a-phase polyvinylidene fluoride films," *Applied Physics Letters*, **98**, pp. 242901-1-3 (2011).
19. Baskaran, S., *et al*., "Strain gradient induced electric polarization in a-phase polyvinylidene fluoride films under bending conditions," *Journal of Applied Physics*, **111**, pp. 014109-1-5 (2012).
20. Mindlin, R. D. and Tiersten, H. F., "Effects of couple-stresses in linear elasticity," *Archive for Rational Mechanics and Analysis*, **11**, pp. 415-448 (1962).
21. Toupin, R. A., "Elastic materials with couple-stresses," *Archive for Rational Mechanics and Analysis*, **11**, pp. 385-414 (1962).
22. Koiter, W. T., "Couple stresses in the theory of elasticity, I and II," *Philosophical Transactions of the Royal Society of London B*, **67**, pp.17-44 (1969).
23. Mindlin, R. D., "Micro-structure in linear elasticity," *Archive for Rational Mechanics and Analysis*, **16**, pp. 51-78 (1964).
24. Yang, F., *et al*., "Couple stress based strain gradient theory for elasticity," *International Journal of Solids And Structures*, **39**, pp. 2731-2743 (2002).
25. Hadjesfandiari, A. R. and Dargush, G. F., "Couple stress theory for solids," *International Journal of Solids And Structures*, **48**, pp. 2496-2510 (2011).
26. Wang, G. F., "A piezoelectric constitutive theory with rotation gradient effects," *European Journal of Mechanics A-Solids*, **23**, pp. 455-466 (2004).
27. Liang, X. and Shen, S. P., "Size-dependent piezoelectricity and elasticity due to the electric field-strain gradient coupling and strain gradient elasticity," *International Journal of Applied Mechanics*, **5**, pp. 1350015-1-16 (2013).
28. Shen, S. P. and Hu, S. L., "A theory of flexoelectricity with surface effect for elastic dielectrics," *Journal of the Mechanics and Physics of Solids*, **58**, pp. 665-677 (2010).
29. Hadjesfandiari, A. R., "Size-dependent piezoelectricity," *International Journal of Solids and Structures*, **50**, pp. 2781-2791 (2013).
30. Yan, Z. and Jiang, L. Y., "Size-dependent bending and vibration behaviour of piezoelectric nanobeams due to flexoelectricity," *Journal of Physics D-Applied Physics*, **46**, pp. 355502-1-7 (2013).
31. Hu, Y. T., *et al*., "The effects of first-order strain gradient in micro piezoelectric-bimorph power harvesters," *IEEE Transactions on Ultrasonics Ferroelectrics and Frequency Control*, **58**, pp. 849-852 (2011).
32. Wang, J. N., *et al*., "On the strain-gradient effects in micro piezoelectric-bimorph circular plate power harvesters," *Smart Materials and Structures*, **21**, pp. 015006-1-6 (2012).
33. Li, A. Q. *et al*., "Size-dependent analysis of a three-layer microbeam including electromechanical coupling," *Composite Structures*, **116**, pp. 120-127 (2014).
34. Zhao, J. and Pedroso, D., "Strain gradient theory in orthogonal curvilinear coordinates," *International Journal of Solids and Structures*, **45**, pp. 3507-3520

https://doi.org/10.1017/jmech.2016.104 Published online by Cambridge University Press

(2008).

35. Zhang, B., *et al*., "A novel size-dependent functionally graded curved microbeam model based on the strain gradient elasticity theory," *Composite Structures*, **106**, pp. 374-392 (2013).
36. Wang, Q., *et al*., "Analysis of piezoelectric coupled circular plate," *Smart Materials & Structures*, **10**, pp. 229-239 (2001).
37. Sekouri, E. M., *et al*., "Modeling of a circular plate with piezoelectric actuators," *Mechatronics*, **14**, pp. 1007-1020 (2004).
38. Wah, T., "Vibration of circular plates," *The Journal of the Acoustical Society of America*, **34**, pp. 275-281 (1962).

(Manuscript received April 29, 2016,
accepted for publication August 29, 2016.)

https://doi.org/10.1017/jmech.2016.104 Published online by Cambridge University Press